INSTITUTE OF PHYSICS PUBLISHING JOURNAL OF PHYSICS B: ATOMIC, MOLECULAR AND OPTICAL PHYSICS

J. Phys. B: At. Mol. Opt. Phys. **34** (2001) 681–697 www.iop.org/Journals/jb PII: S0953-4075(01)19093-0

Electron-impact excitation of Fe^{20+}, including $n = 4$ levels

N R Badnell[1] **and D C Griffin**[2]

[1] Department of Physics and Applied Physics, University of Strathclyde, Glasgow G4 0NG, UK
[2] Department of Physics, Rollins College, Winter Park, FL 32789, USA

Received 15 November 2000, in final form 16 January 2001

Abstract

We have carried out a 200 level close-coupling calculation for C-like Fe using the R-matrix method in conjunction with the intermediate coupling frame transformation method. We have generated effective collision strengths over $T = 8 \times 10^4$–8×10^7 K for all 19 900 inelastic transitions, which is an order of magnitude larger than has been generated hitherto. We provide illustrative comparisons with the results of previous workers, where possible, and find a broad accord. The consistent and comprehensive set of data that we have generated (energy levels, radiative rates and effective collision strengths) is necessary for the collisional–radiative modelling of metallic impurities that will arise in the next generation of magnetic fusion reactors as well as being of relevance to studies utilizing observations from the high-resolution x-ray satellites *Chandra* and *XMM–Newton*.

1. Introduction

Iron is arguably the most important astrophysical element, from a spectroscopic diagnostic point of view. As such, it has been the subject of a vast number of theoretical studies into its electron collisional properties, namely ionization and recombination (for ionization balance) and excitation (for level populations). Most notably, the IRON Project (Hummer *et al* 1993) aims to calculate electron-impact excitation rate coefficients for every ionization stage of iron using the R-matrix method. Most of their effort has been directed to the Breit–Pauli R-matrix approach (Scott and Burke 1980), which can be expected to give accurate and reliable results, but is computationally demanding. An alternative approach is to use the LS-coupling R-matrix method (including the mass–velocity and Darwin operators) in conjunction with the intermediate coupling frame transformation (ICFT) method (Griffin *et al* 1998) to take account of spin–orbit effects. Such an approach is much less computationally demanding than the equivalent-sized full Breit–Pauli approach while being just as accurate, for all practical purposes (Griffin and Badnell 2000). This enables data to be computed more rapidly or larger-scale calculations to be attempted. The ICFT method can also be used in conjunction with new R-matrix methods and codes that, currently, only exist in non-relativistic forms such as RMATRX II (Burke *et al* 1994).

0953-4075/01/040681+17$30.00

It is the aspect of large-scale calculations which is the subject of this paper, which is also an RmaX Network[1] publication. Following-on from the IRON Project, the RmaX Network aims to calculate R-matrix atomic data for x-ray processes which, for example, will be of relevance to studies utilizing observations from the high-resolution x-ray satellites *Chandra* and *XMM–Newton*. This involves not just data for Fe and Fe-like elements but for C, N, O, Ne etc as well, and for photoionization as well as for electron-impact excitation. It is the focus on x-ray transitions which sets the work of the RmaX Network apart from that of the IRON Project. Another motivation for this paper is the next generation of magnetic fusion devices which aim to test reactor operation under conditions nearer to those required for long-term power generation. More durable materials will be used and will see a return to the greater use of Fe/Ti/Ni etc, as well as new metals, namely W/Ta. This is to be contrasted with current test-reactors which make greater use of lightweight, but less durable, materials such as Be/C. With greater control now available over impurities, using divertors etc, the historical poisoning of the fusion plasma by strongly radiating (i.e. high Z) elements is less of an issue and the engineering advantage of metals takes precedence. However, the electron densities can be upwards of 10^{16} cm^{-3} where the coronal assumption made of many astrophysical plasmas is not valid and full collisional–radiative modelling becomes necessary. This in turn requires a more comprehensive treatment of collision processes since a great many excitations contribute to level populations, both directly and indirectly. Thus, it is desirable to be able to generate as comprehensive a set of accurate, i.e. R-matrix, data as possible. The ICFT approach enables us to generate an order of magnitude more data than is possible with a full Breit–Pauli R-matrix calculation.

Before we focus on the problem at hand, we note that an alternative approach to larger-scale Breit–Pauli R-matrix calculations has been introduced recently by Pelan and Berrington (2001). They divide a set of close-coupling (CC) levels into two groups, a 'low-lying' one and a 'high-lying' one. They carry out a low-energy, low angular momentum, Breit–Pauli R-matrix calculation through the resonance region using the full CC set of levels and then a second one, to much higher energies and angular momentum, that retains only the low-lying set of levels in the CC expansion. By restricting the use of the full CC set to low energies only, they require only a relatively small continuum basis expansion and this renders the problem tractable. In particular, cross sections for transitions between the low-lying set of levels contain resonances attached to levels from the high-lying set. Above the ionization limit, the effect of continuum-coupling of the high-lying set of levels on the low-lying set is small for sufficiently highly-charged ions and they can be omitted from the CC expansion enabling the number of continuum basis orbitals to be increased. This is necessary so as to be able to calculate cross sections for the low-lying set of levels to sufficiently high energy (and angular momentum) so as to be able to generate rate coefficients. One advantage of the ICFT method is that it can carry out calculations of the same size as the full CC set of Pelan and Berrington (2001) but to a high enough energy and angular momentum so as to be able to generate rate coefficients for transitions between *all* levels of the full CC set. Also, since the full CC set is retained throughout, the ICFT method can be applied to low charge-state ions where coupling between the low- and high-lying sets cannot be neglected.

Electron-impact excitation of C-like Fe^{20+} has been considered by Butler and Zeippen (2000) as part of the IRON Project and they provide a comprehensive survey of prior work, which their results largely supersede. Of particular note is the work by Phillips *et al* (1996). They only carried out distorted-wave calculations but these included transitions of the form $2\mathrm{p} \rightarrow n\mathrm{s}, \mathrm{d}$ ($n = 4, 5$) relevant to diagnosing soft x-ray flares. Zhang and Sampson (1996,

[1] Available at http://amdpp.phys.strath.ac.uk/UK_RmaX.

1997) have carried out much more extensive calculations (in terms of $n = 3$ levels) than Butler and Zeippen (2000) but only provide ordinary (energy-dependent) collision strengths calculated in the distorted-wave approximation. The effect of resonance contributions on effective collision strengths is so large that even the results of Dirac–Fock R-matrix calculations by Aggarwal (1991), which just included the 20 $n = 2$ levels, can be a serious underestimate due to the omission of resonances attached to $n = 3$ levels (see Butler and Zeippen (2000)). Finally, we note a recent 46CC level Dirac–Fock R-matrix calculation by Aggarwal and Keenan (1999), but they only provide ordinary collision strengths for a subset of transitions and only above the ionization limit. There is no obvious physical reason why a Dirac–Fock approach should be necessary for $Z = 26$. The Breit–Pauli approximation should be valid here and be dominated by the one-body operators.

The most comprehensive and reliable results to-date for Fe^{20+}, especially for application purposes, are those of Butler and Zeippen (2000). They carried out a 52CC level Breit–Pauli R-matrix calculation and provided effective collision strengths for all 1326 inelastic transitions. Essentially, they allowed for $2p \rightarrow 3l$ promotions out of the ground configuration, as well as including all levels from the $n = 2$ complex of course. In this paper, in addition, we allow for all $2s \rightarrow 3l$ and $2p \rightarrow 4l$ promotions out of the ground configuration. Correspondingly, this also allows, for example, for $2p \rightarrow 3l$ promotions out of the first excited configuration ($2s2p^3$). This leads us to a 200CC level ICFT R-matrix calculation from which we provide effective collision strengths for all 19 900 inelastic transitions.

The structure of this paper is as follows: in section 2 we discuss our methodology, with particular emphasis on issues that arose in handling the current large-scale ICFT calculations. In section 3, we discuss details of the specific application of our methodology to Fe^{20+}, including results for both energy levels and oscillator strengths. In section 4, we present illustrative results for both ordinary and effective collision strengths and comment on the comparison with the results of Butler and Zeippen (2000), Aggarwal (1991) and Phillips *et al* (1996). We finish with a short conclusion.

2. Methodology

Our basic approach to the solution of the collision problem is to use the R-matrix method (Burke and Berrington 1993) in conjunction with the ICFT method (Griffin *et al* 1998). A complete solution, in terms of reactance or scattering (collision) matrices, is obtained first in LS-coupling. In particular, use is made of multi-channel quantum defect theory (MQDT) to obtain 'unphysical' collision matrices (Gorczyca and Badnell 2000). These are then transformed, first, algebraically to jK-coupling and then, via the use of term-coupling coefficients, to intermediate coupling. Such an approach is typically an order of magnitude less demanding of computer resources than the equivalent full Breit–Pauli R-matrix calculation. Furthermore, the transformation of the 'unphysical' collision matrices ensures that accurate results are obtained in the resonance region.

We now comment on a few pertinent aspects of the methodology. Firstly, it is more efficient to work with (interpolate, close-off etc) the unphysical reactance matrix when, roughly, more than half of the target levels are closed but to work with the unphysical scattering matrix when, roughly, more than half of the target levels are open. On the face of it, the latter is always more efficient since it takes the same number of operations to close-off the scattering matrix as it does the reactance matrix, and the reactance matrix still has to be converted to the scattering matrix. However, in the absence of radiation damping, the reactance matrix is real while the scattering

matrix is complex. The 'inversion' of a real matrix[2] is computationally more efficient than a complex one and when the majority of levels are closed it is the closing-off of the unphysical matrix that dominates the computational time (not the conversion from reactance to scattering matrix) and so the reactance matrix route is more efficient.

Changing from closing-off the unphysical reactance matrix to closing-off the unphysical scattering matrix can have an effect on the continuity of the collision strength as a function of energy when term-coupling coefficients are being used. In general, our LS-coupling CC expansion is smaller than the corresponding configuration interaction (CI) expansion. But our levels are expanded in terms of term-coupling coefficients for all terms in the CI expansion. Those components corresponding purely to CI terms, which should be small, are zeroed-out and the remaining components are normally just renormalized to unity. However, this does not ensure a unitary transformation from jK-coupling to intermediate coupling. If the (unphysical) reactance matrix is transformed (and closed-off) then the subsequent conversion to the (physical) scattering matrix re-imposes unitarity. If the unphysical scattering matrix is transformed (and closed-off) then the resulting physical scattering matrix is no longer unitary. This gives rise to 'small' differences in the collision strength calculated via each scheme and to a discontinuity on switching from one to the other. We eliminate this discrepancy by re-*ortho*normalizing the term-coupling coefficients, following the zeroing-out of some components, and this ensures a unitary transformation to intermediate coupling and the elimination of the discontinuity.

Finally, in the case of highly-charged ions, it is generally true that the set of levels arising from a set of CC terms cannot be expanded in terms of term-coupling coefficients arising solely from the CC terms. Instead, there will be non-negligible components from energetically adjacent CI terms, of the appropriate symmetry. In the past we have identified a set of CC levels that we want collision data for and have included all of the CC terms necessary to represent these levels. This usually gives rise to additional levels, that are not well represented by the term-coupling coefficient components retained, and to associated collision data (collision strengths etc) which should be ignored and/or discarded. This is inefficient since the most time consuming part of an ICFT R-matrix calculation is concerned with the operations involving the level-resolved collision matrices. Within reason, we can increase the number of CC terms in the LS-coupling calculation without impacting unduly upon the overall computational effort, provided that these additional terms are not used to construct additional CC levels. In other words, we now allow for the case where the number of levels (that could be) constructed from the (LS) CC terms can be larger than the number of CC levels defined by the term-coupling coefficients, and for which we ultimately provide collision data. Since the operation count for the ICFT method is an N^3 process in the number of CC levels, we are not forced to unduly restrict the size of the LS-coupling CC expansion on the grounds that it will give rise to too large a CC level expansion.

3. Application to Fe^{20+}

3.1. Structure

In table 1, we list the 24 configurations that make up our CI expansion. These give rise to 268 terms and 564 levels. The 200 levels included in our CC expansion are all of those that arise from configurations 1–9 and 13–16, plus the lowest two levels of configuration 10. The energy levels are shown in figure 1. The solid lines denote CC levels while dashed lines denote purely CI levels. The $n = 2$ configurations (1–3) are well separated from the

[2] Of course, we actually solve $Ax = b$ rather than $x = A^{-1}b$.

Table 1. Configurations included for Fe^{20+}.

1	$2s^22p^2$	2	$2s2p^3$	3	$2p^4$		
4	$2s^22p3s$	5	$2s^22p3p$	6	$2s^22p3d$		
7	$2s2p^23s$	8	$2s2p^23p$	9	$2s2p^23d$		
10	$2p^33s$	11	$2p^33p$	12	$2p^33d$		
13	$2s^22p4s$	14	$2s^22p4p$	15	$2s^22p4d$	16	$2s^22p4f$
17	$2s2p^24s$	18	$2s2p^24p$	19	$2s2p^24d$	20	$2s2p^24f$
21	$2p^34s$	22	$2p^34p$	23	$2p^34d$	24	$2p^34f$

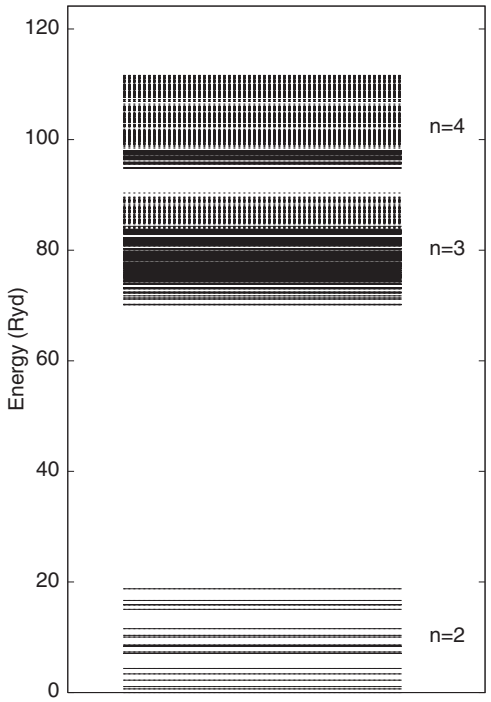

Figure 1. Energy level representation for Fe^{20+}. The solid lines denote CC levels and the broken lines purely CI levels. The upper bounding box delineates the ionization limit.

$n = 3$ (4–12) and $n = 4$ (13–24) configurations. The latter two sets, although much closer in energy, do not overlap. However, we see that the $n = 4$ configurations that we include in our CC expansion (13–16) lie above some of the $n = 3$ configurations that we omit from it (part of 10, plus 11 and 12). We argue that this is a reasonable approach. These $n = 4$ configurations are of the form $1s^22s^22p4l$ ($l = 0$–3) and are there to allow for 2p promotions from the important ground configuration $1s^22s^22p^2$. The omitted $n = 3$ levels are from configurations of the form $1s^22p^33l$ ($l = 0$–2) which differ from them by two or three electrons and so cannot couple directly to them. The omission of some $n = 3$ levels from the CC expansion also affects the highest $n = 3$ levels retained, but really only through continuum coupling. The omitted and retained levels are too close in energy for any significant resonances attached to the former to be energetically accessible to the latter. To include the additional 76 $n = 3$ levels in our CC expansion would be tedious with our current workstation processors (333 MHz UltraSparc II) as the present calculations took about 500 CPU hours on them. However, CPU memory (400 Mb) and disk space (10 Gb) are not an issue with the ICFT approach.

Table 2. Potential scaling parameters λ_{nl} used for Fe^{20+}.

1s	1.379 88	3s	1.384 80	4s	1.327 21
2s	1.250 35	3p	1.258 30	4p	1.254 40
2p	1.183 59	3d	1.396 90	4d	1.371 30
				4f	1.445 40

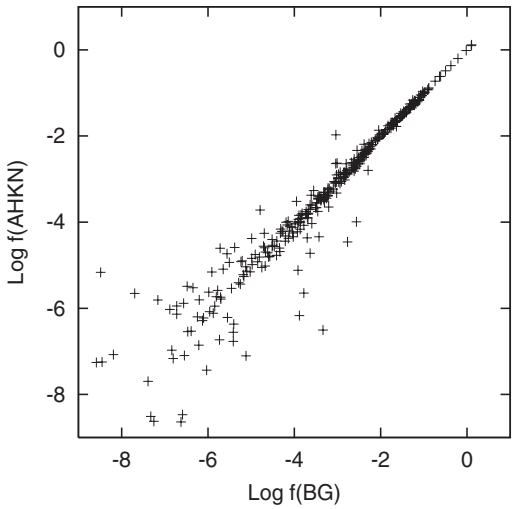

Figure 2. Absorption oscillator strengths for Fe^{20+}. AHKN denotes those of Aggarwal *et al* (1997) and BG denotes this work.

We used AUTOSTRUCTURE (Badnell 1986, 1997) to generate our atomic structure and, hence, the radial orbitals for the R-matrix calculation. We used nl-dependent scaling parameters for the Thomas–Fermi–Dirac–Amaldi statistical potential, as given in table 2. The 1s, 2s and 2p scaling parameters were optimized simultaneously by minimizing the equally-weighted sum of all term energies arising from the $n = 2$ configurations (1–3). The $3l$ and $4l$ scaling parameters were each optimized on a single configuration ($1s^2 2s^2 2p nl$) by minimizing the equally-weighted sum of all term energies arising from said configuration.

In table 3, we compare the energies of our lowest 56 levels with those resulting from large CI calculations with CIV3 by Aggarwal *et al* (1997) and from a 46 level calculation with GRASP by Aggarwal and Keenan (1999), as well as with observed values (Corliss and Sugar 1982). We see that the agreement is more than satisfactory.

Butler and Zeippen (2000, table 2) used SUPERSTRUCTURE to generate energy levels for Fe^{20+}, but obtained much poorer agreement with the observed values. It now appears that these results are not quite correct (Butler 2000). However, the effective collision strengths generated by Butler and Zeippen (2000) are unaffected since the R-matrix calculation re-calculates the atomic structure using only the tabulated radial functions from SUPERSTRUCTURE.

We compared our energy levels calculated using AUTOSTRUCTURE with those that we obtained from the N-electron R-matrix structure calculation. The two differed by less than 2×10^{-6} Ryd, provided that we switched-off the two-body fine and non-fine structure operators in AUTOSTRUCTURE and ensured that the R-matrix calculation used the same Blume and Watson screening parameters as AUTOSTRUCTURE.

Table 3. Some energy levels (Ryd) of Fe^{20+}.

Index	Configuration	Level	Observed[a]	AS[b]	CIV3[c]	GRASP[d]
1	$2s^22p^2$	$^3P_0$	0.0	0.0	0.0	0.0
2	$2s^22p^2$	$^3P_1$	0.6730	0.6615	0.6599	0.6739
3	$2s^22p^2$	$^3P_2$	1.0694	1.0867	1.0634	1.0760
4	$2s^22p^2$	$^1D_2$	2.2286	2.2469	2.2383	2.2480
5	$2s^22p^2$	$^1S_0$	3.3890	3.3898	3.4820	3.3598
6	$2s2p^3$	$^5S_2$	4.4374	4.3524	4.3979	4.3184
7	$2s2p^3$	$^3D_1$	7.0785	7.0723	7.1098	7.0934
8	$2s2p^3$	$^3D_2$	7.0837	7.0829	7.1166	7.1007
9	$2s2p^3$	$^3D_3$	7.3259	7.3507	7.3538	7.3328
10	$2s2p^3$	$^3P_0$	8.3507	8.3420	8.3859	8.3650
11	$2s2p^3$	$^3P_1$	8.4281	8.4325	8.4623	8.4479
12	$2s2p^3$	$^3P_2$	8.5870	8.6043	8.6210	8.6076
13	$2s2p^3$	$^3S_1$	9.9838	10.030	10.035	10.137
14	$2s2p^3$	$^1D_2$	10.268	10.343	10.338	10.414
15	$2s2p^3$	$^1P_1$	11.491	11.558	11.560	11.641
16	$2p^4$	$^3P_2$	15.002	15.055	15.129	15.153
17	$2p^4$	$^3P_0$	15.817	15.857	15.940	15.974
18	$2p^4$	$^3P_1$	15.861	15.894	15.973	15.999
19	$2p^4$	$^1D_2$	16.560	16.657	16.704	16.774
20	$2p^4$	$^1S_0$	18.665	18.771	18.836	18.911
21	$2s^22p3s$	$^3P_0$		70.117	70.129	70.178
22	$2s^22p3s$	$^3P_1$		70.206	70.216	70.250
23	$2s^22p3s$	$^3P_2$		71.125	71.137	71.263
24	$2s^22p3s$	$^1P_1$		71.366	71.383	71.476
25	$2s^22p3p$	$^3D_1$		71.749	71.744	71.794
26	$2s^22p3p$	$^1P_1$		72.264	72.263	72.355
27	$2s^22p3p$	$^3D_2$		72.295	72.290	72.341
28	$2s^22p3p$	$^3P_0$		72.448	72.432	72.581
29	$2s^22p3p$	$^3P_1$		72.997	72.995	73.181
30	$2s^22p3p$	$^3D_3$		73.085	73.090	73.207
31	$2s^22p3p$	$^3S_1$		73.185	73.189	73.355
32	$2s^22p3p$	$^3P_2$		73.239	73.226	73.417
33	$2s2p^23s$	$^5P_1$		73.821		
34	$2s^22p3p$	$^1D_2$		73.821	73.804	73.936
35	$2s^22p3d$	$^3F_2$		73.943	73.733	73.896
36	$2s2p^23s$	$^5P_2$		74.261		
37	$2s^22p3d$	$^3F_3$	73.825	74.296	74.081	74.245
38	$2s^22p3d$	$^3D_2$	74.609	74.362	74.136	74.315
39	$2s^22p3p$	$^1S_0$		74.382	74.371	74.514
40	$2s^22p3d$	$^3D_1$		74.529	74.312	74.486
41	$2s2p^23s$	$^5P_3$		74.718		
42	$2s2p^23s$	$^3P_0$		74.872		
43	$2s^22p3d$	$^3F_4$		75.019	74.809	75.042
44	$2s^22p3d$	$^1D_2$	73.794	75.092	73.873	75.126
45	$2s2p^23s$	$^3P_1$		75.197		
46	$2s^22p3d$	$^3D_3$	74.831	75.308	75.092	75.334
47	$2s^22p3d$	$^3P_0$		75.420	75.237	75.498
48	$2s^22p3d$	$^3P_1$		75.421	75.218	75.477
49	$2s^22p3d$	$^3P_2$	75.005	75.432	75.214	75.469
50	$2s2p^23p$	$^5D_0$		75.531		

Table 3. (Continued)

Index	Configuration	Level	Observed[a]	AS[b]	CIV3[c]	GRASP[d]
51	$2s2p^23p$	$^5D_1$		75.556		
52	$2s2p^23s$	$^3P_2$		75.678		
53	$2s2p^23p$	$^5D_2$		75.864		
54	$2s2p^23p$	$^3S_1$		75.893		
55	$2s^22p3d$	$^1F_3$	75.642	75.999	75.772	76.007
56	$2s^22p3d$	$^1P_1$	75.577	76.002	75.776	76.027

[a] Corliss and Sugar (1982).
[b] AUTOSTRUCTURE (this paper).
[c] Aggarwal *et al* (1997).
[d] Aggarwal and Keenan (1999).

In figure 2, we compare our absorption oscillator strengths with those of Aggarwal *et al* (1997) which they obtained using CIV3. There is a distinct reduction in the spread compared to that observed by Butler and Zeippen (2000, figure 1) because their tabulated oscillator strengths are also somewhat inaccurate (Butler 2000).

3.2. Collision

We carried out LS-coupling inner-region R-matrix calculations, including the mass–velocity and Darwin operators, using codes that were originally based on the published exchange (Berrington *et al* 1995) and non-exchange (Burke *et al* 1992) R-matrix codes. We used a 112CC term expansion consisting of the 100 terms necessary to generate the pure 200CC level expansion discussed above plus an additional 12 terms that gave rise to components in the term-coupling coefficient expansion that were larger than 0.01. The level-resolved collision matrix elements for the additional resultant 28 levels did not need to be computed. In addition, since our LS-coupling CC expansion is smaller than our CI expansion, we necessarily constructed a balanced 'correlation' expansion following Gorczyca *et al* (1995). The outer-region solutions were obtained using our MQDT version of Seaton's unpublished STGF code; this treats all closed channels as 'open' (Gorczyca and Badnell 2000). The ICFT calculation was made with our unpublished STGICF and STGICFDAMP codes for working with the unphysical reactance and scattering matrices, respectively.

We carried out our exchange calculations up to $J = 21/2$ and our non-exchange calculations thereon up to $J = 75/2$. The 'top-up' contribution (from higher J) for dipole transitions was computed using the Burgess (1974) sum rule. We took care to check for numerical failure in the generation of the Coulomb integrals by comparing the numerical result with its analytic asymptotic form (Burgess *et al* 1970). Coulomb integrals for transitions between widely-spaced energy levels can become vanishingly small while, at the same time, those for transitions between closely-spaced levels can remain non-negligible. Numerical failure inevitably occurs when the energy separation becomes large enough because the integral series expansion cannot be accurately computed using a finite machine representation for real numbers. However, it is easy to examine the parameter space of energy and angular momentum and to show that the Coulomb integrals are well represented by their asymptotic form before numerical failure occurs, and this is what is used instead. In addition, the top-up contribution for non-dipole transitions was computed assuming a geometric series in energy and taking care to switch-over smoothly to the degenerate-energy limiting case (Burgess *et al* 1970). We compared the summed collision strength with top-up to that without top-up at every energy and for every transition. The top-up contribution was at most a few per cent for the dipole

transitions while for the non-dipole transitions the maximum top-up was less than 30% of the total, with only a handful being in the 20–30% range. This latter case occurred, typically, for weak transitions.

We used 24 continuum basis orbitals initially[3], the number being progressively reduced automatically in the non-exchange calculations as the scattering angular momentum increased. This enabled us to calculate total collision strengths explicitly up to 400 Ryd. For dipole transitions, collision strengths were calculated at higher energies by interpolating the reduced collision strength, as a function of reduced scattering energy, between the values up to 400 Ryd and the infinite energy limit-point, following Burgess and Tully (1992). The non-dipole collision strengths were extrapolated as a constant in energy. We actually observe a range of behaviours, namely according to $E^{-\alpha}$, with $\alpha = 0$–2. By comparing effective collision strengths for selected transitions that were computed using the correct energy behaviour for the collision strength with those that were computed assuming the collision strength to be constant in energy, we were able to determine the maximum temperature that we could accurately tabulate these effective collision strength for. In principle, one could determine all of the high energy behaviours, but this would best done by making use of the infinite energy Born limit (Burgess *et al* 1997). For now, we can accurately tabulate all effective collision strengths up to $\log_{10}(T(\mathrm{K})) = 7.6$, at which temperature the coronal fractional abundance of Fe^{20+} is less than 10^{-4} (Arnaud and Raymond 1992). By the ADAS *adf04* temperature given by $\log_{10}(T(\mathrm{K})) = 7.9$, results for a few of the non-dipole transitions may be subject to increasing extrapolation error ($\sim$20%). However, it is likely that only the dipole transitions may still be of interest at these high temperatures.

The low-temperature limit of our effective collision strength tabulation follows from the fact that the vast majority of the energy levels have not been observed. Low-temperature effective collision strengths are sensitive to the presence and/or absence of resonances just above each threshold, along with their resolution. We carried out two calculations of collision strengths through the $n = 2$ thresholds, one using our calculated level energies and one using the observed. We then compared the effective collision strengths. Differences of more than a factor of two were noted at temperatures below 10^6 K for some transitions. Given the uncertainty in the value of the calculated $n > 2$ level energies, we set our lowest recommended temperature for transitions involving these levels to be $\log_{10}(T(\mathrm{K})) = 6.2$. It should be noted that errors of 30% are still possible at this temperature, but these rapidly diminish with increasing temperature. Again, from Arnaud and Raymond (1992), the coronal fractional abundance is small ($<10^{-5}$) for $\log_{10}(T(\mathrm{K})) < 6.2$. The situation for a photoionized plasma is somewhat different, a significant fractional abundance persists to lower temperatures, and so effective collision strengths are required to lower electron temperatures. However, the lower electron temperature means that it is transitions between low-lying (e.g. $n = 2$) levels that are the most important. Since we have used the observed $n = 2$ level energies in our calculations, our effective collision strengths amongst the $n = 2$ levels can be extended to lower temperatures and we tabulate them down to the ADAS *adf04* temperature given by $\log_{10}(T(\mathrm{K})) = 4.9$.

Resolution of the resonance structure becomes increasingly laborious as the residual charge-state (z) of an ion increases. This is because the energy separation between principal quantum shells, and hence the energy spread of resonances, scales as z^2, while the autoionizing width is independent of z; i.e. the number of energy points should increase as z^2 so as to maintain the same level of resolution. Based on sample calculations, we chose to use an energy step of $1 \times 10^{-5} z^2$ Ryd through energy regions where $\delta n = 0$ resonances were present and a

[3] An equivalent full Breit–Pauli R-matrix calculation would have necessitated the diagonalization of $(N+1)$-electron Hamiltonian matrices of the order of 25 000 since the number of level-resolved channels is just over 1000. Matrices of this size (>1000) still have to be manipulated by STGICF and/or STGICFDAMP though.

step of $4 \times 10^{-5} z^2$ Ryd where only $\delta n = 1$ resonances were present. Finally, we used a step of $0.01 z^2$ Ryd above all thresholds. This resulted in a total of 13 027 energies being used. Although this energy mesh is sufficient to resolve the dominant resonance structure, a large number of weaker resonances are only partially resolved. A step of $\sim 10^{-9} z^2$ Ryd for $\delta n = 0$ resonances and a step of $\sim 10^{-7} z^2$ Ryd for $\delta n = 1$ resonances would be required before narrower resonances could be assumed to be significantly radiation damped. We have taken care to try to eliminate all sources of numerical failure in the computation of the collision strengths, e.g. the evaluation of MQDT functions with perturbations, deeply-closed channels, near threshold problems, top-up, etc. The point of all this is to enable us to make use of a statistical argument for retaining partially resolved resonances in the determination of the effective collision strength. Consider a model problem where, say, one has 100 resonances each of the same width which is a factor of 10 smaller than the energy step being used to map them out. On average one would 'hit' one in ten resonances, at a single point. But the strength of that resonance would be overestimated by a factor of 10—compare the area of the 'triangle' with that obtained by integrating over a Lorentz profile. Thus, the over- and under-estimates are largely self-cancelling. Such an argument fails when only a small number of partially resolved resonances contribute, e.g. at low temperatures, or where there is large-scale numerical failure in computing the collision strength.

We examined the value of the collision strength for every transition (19 900 of them) at every energy in the resonance region ($\approx$13 000 of them) and found 297 data points for which the collision strength differed by a factor of 1000 or more from the value of the point at either side, while $\approx$11 000 of them differed by a factor of 100 or more. This is to be compared with the total number of data points $\sim$100 million. On investigating certain transitions more closely, using a finer energy mesh over a limited energy range, we did indeed observe a large amount of self-cancellation between the over- and under-estimate of the integrated collision strength from partially-resolved resonances. Given that the 297 data points represent the most extreme range of the statistics and the ones most likely to be subject to any numerical failure, we chose to eliminate (only) those points. The only effective collision strengths significantly affected (by more than a factor of 1.5) by this procedure were those for 20 transitions which were between levels which differ by two electrons.

4. Results

Our 200CC level calculation gives rise to a large amount of data, e.g. effective collision strengths for 19 900 transitions, and so we only present some illustrative results for comparison here. The full set of results for energy levels, dipole radiative rates and effective collision strengths, tabulated in the ADAS *adf04* format (Summers 1994, 1999), is available via the WWW under http://www-cfadc.phy.ornl.gov/data_and_codes. The effective collision strengths (Seaton 1953) are tabulated over $\log_{10}(T(\mathrm{K})) = 4.9$–$7.9$[4] which comfortably exceeds the temperature of peak coronal fractional abundance (10^7 K) for Fe^{20+} and spans the lower temperatures of interest to photoionized plasmas.

4.1. $n = 2$ to $n' = 2$

For transitions amongst levels of the ground configuration, we would not expect any significant differences from the results of Butler and Zeippen (2000) since they allowed for the dominant $2\mathrm{p} \rightarrow 3l$ promotions here. In figure 3(*a*) we show the collision strength for the transition (2–3):

[4] But, bear in mind the caveats given in section 3.2 and which are repeated in the *adf04* file.

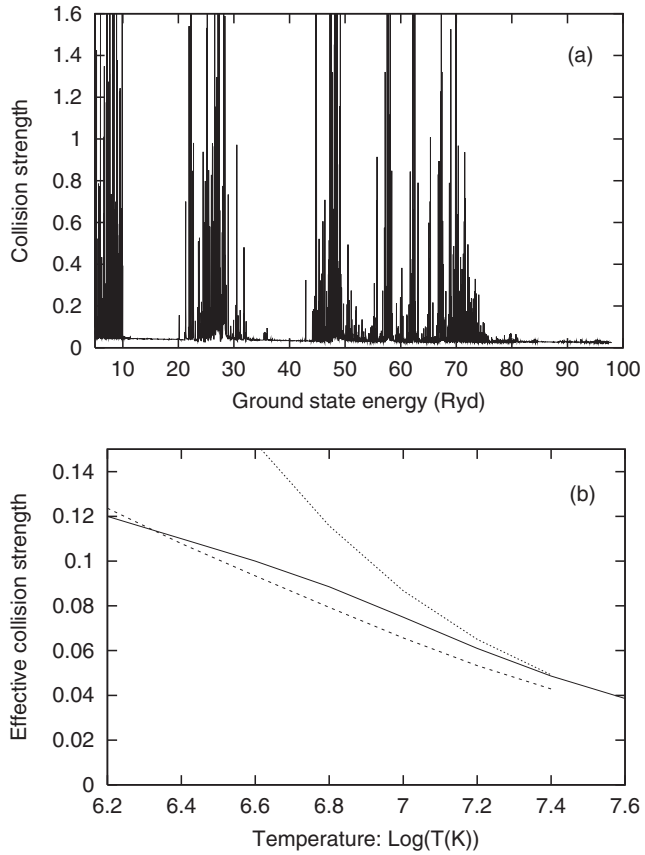

Figure 3. Transition (2–3): $2s^2 2p^2\ ^3P_1$–$2s^2 2p^2\ ^3P_2$. (*a*) Collision strength versus energy relative to the Fe^{20+} ground state (this paper). (*b*) Effective collision strengths: solid curve, this paper; dashed curve, Butler and Zeippen (2000); dotted curve, Aggarwal (1991).

$2s^2 2p^2\ ^3P_1 - {}^3P_2$ and note little qualitative difference from that of Butler and Zeippen (2000, figure 4). This is confirmed by a comparison of the effective collision strengths in figure 3(*b*). There is only a modest increase at 10^7 K which can be attributed to the $2s \rightarrow 3l$ and $2p \rightarrow 4l$ promotions that are also allowed for by our calculations. The results of Aggarwal (1991), who carried out a Dirac–Fock calculation including only the $n = 2$ levels, differ markedly at low temperatures. We observe a similar behaviour for a number of other transitions as well. (Also, the Dirac–Fock results of Aggarwal *et al* (2000) for Fe^{14+} show a similar trend, the low temperature effective collision strengths being significantly larger than those of the Breit–Pauli *R*-matrix results of Eissner *et al* (1999) and the ICFT *R*-matrix results of Griffin *et al* (1999).) Aggarwal (1991) used 2871 energy points to span the range of the $n = 2$ thresholds. We used 4701 points here and observed little sensitivity to using a finer energy mesh. The only sensitivity that we observed was to the positioning of near-threshold resonances, but this should not lead to one set of results being consistently larger than another.

For transitions between levels of the ground and the first excited configuration, we can observe larger qualitative differences between our collision strengths and those of Butler and Zeippen (2000). In figure 4(*a*) we show the collision strength for the transition (4–8): $2s^2 2p^2\ ^1D_2$–$2s2p^3\ ^3D_2$. The resonance structure above 60 Ryd is largely absent from the results of

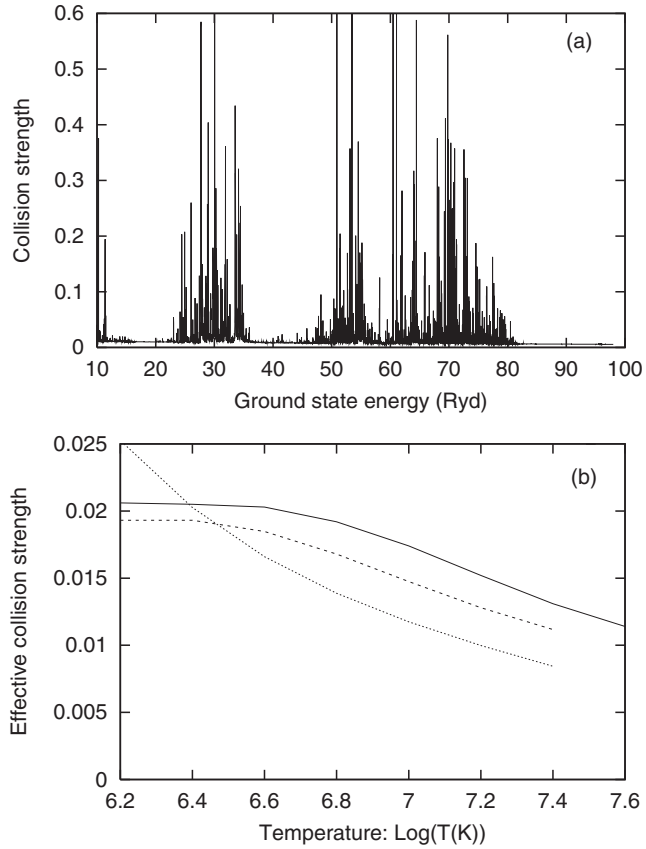

Figure 4. Transition (4–8): $2s^2 2p^2\ {}^1D_2$–$2s2p^3\ {}^3D_2$. (*a*) Collision strength versus energy relative to the Fe^{20+} ground state (this paper). (*b*) Effective collision strengths: solid curve, this paper; dashed curve, Butler and Zeippen (2000); dotted curve, Aggarwal (1991).

Butler and Zeippen (2000, figure 6). However, this does not lead to a significant difference in the effective collision strength, as shown in figure 4(*b*). On the other hand, if we consider a weaker transition (1–14): $2s^2 2p^2\ {}^3P_0$–$2s2p^3\ {}^1D_2$, then the strong resonance structure above 60 Ryd observed in figure 5(*a*) does now translate into a larger (factor of 2) effective collision strength, as seen in 5(*b*).

For transitions between levels of the first excited configuration, our inclusion of the $2s2p^2 3l$ configurations allows for the dominant $2p \rightarrow 3l$ promotions. In figure 6(*a*) we show the collision strength for the relatively strong transition (7–8): $2s2p^3\ {}^3D_1$–$^3D_2$ and note that the resonances above 60 Ryd lead to a 30% increase in the effective collision strength at 10^7 K, as seen in figure 6(*b*).

4.2. $n = 2$ to $n' = 3$

For these transitions, the scattered energy is much smaller in the $n = 3$ and 4 resonance regions (compared to that for $n = 2$ to 2 transitions) and so the resonant enhancement of the effective collision strength is peaked at much lower temperatures, where the coronal fractional abundance of Fe^{20+} can be expected to be small. We illustrate this in figure 7 for the transition

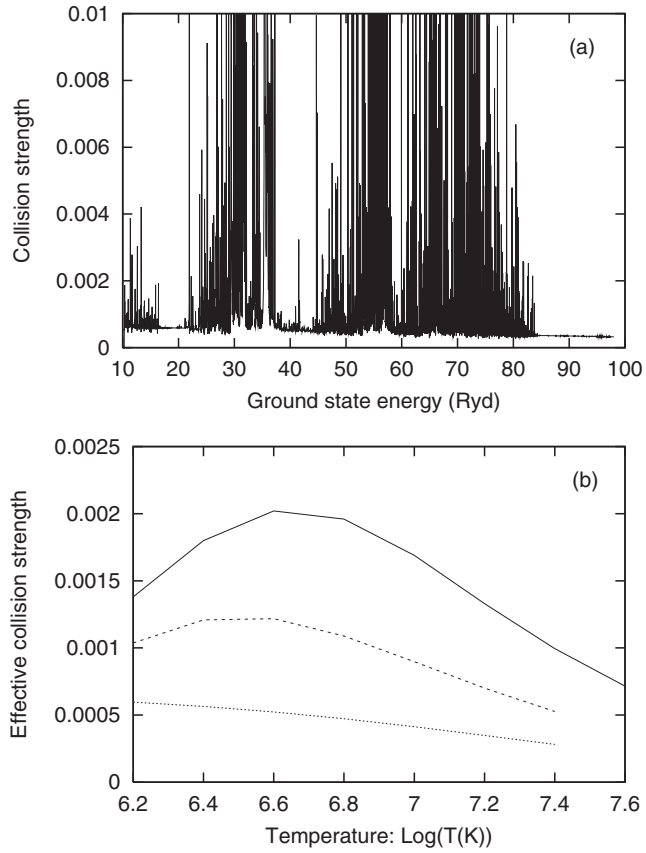

Figure 5. Transition (1–14): $2s^22p^2\ ^3P_0$–$2s2p^3\ ^1D_2$. (*a*) Collision strength versus energy relative to the Fe^{20+} ground state (this paper). (*b*) Effective collision strengths: solid curve, this paper; dashed curve, Butler and Zeippen (2000); dotted curve, Aggarwal (1991).

(1–21): $2s^22p^2\ ^3P_0 - 2s^22p3s\ ^3P_0$. Being a relatively weak transition, there is still a 30% difference in the effective collision strength between our results and those of Butler and Zeippen (2000) at 10^7 K (63 Ryd). Although the highest $n = 3$ threshold lies at 15 Ryd on the energy scale of figure 7, the weak resonance structure observed at higher energies is not the only contribution from resonances attached to the $2s^22p4l$ configurations. In fact, these extend all the way down to about zero (scattered) energy.

An interesting class of transitions arise from the first excited configuration, namely $2s2p^3 \rightarrow 2s^22p3l$. These involve a two-electron jump and so the direct (i.e., non-resonant) collision strength can be expected to be small. However, they can proceed via two sequential (core) one-electron jumps via intermediate resonance states of the form $2s2p^23lnl'$. We illustrate the results for such a transition (7–22): $2s2p^3\ ^3D_1$–$2s^22p3s\ ^3P_1$ in figure 8. The effective collision strength of Butler and Zeippen (2000) is barely distinguishable from zero on this scale.

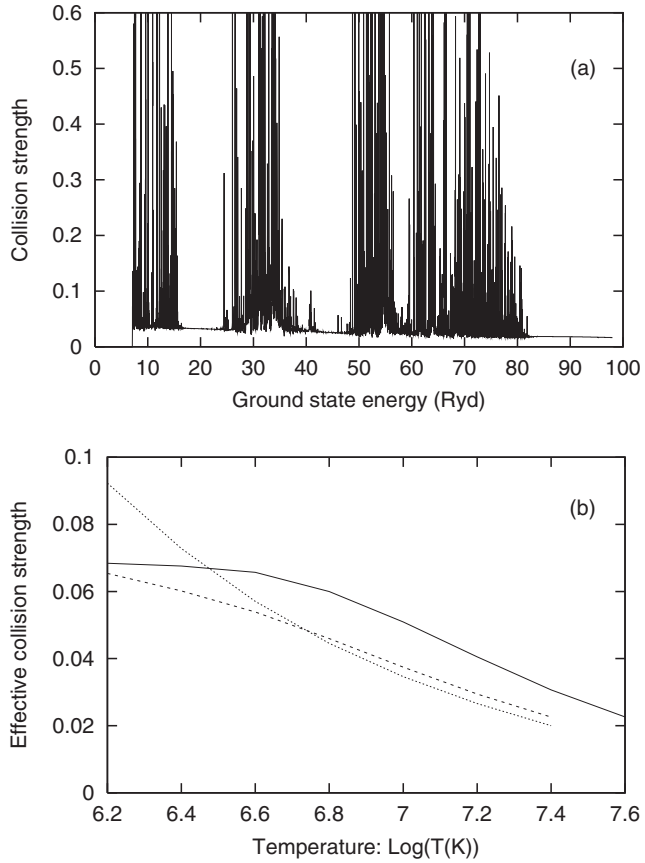

Figure 6. Transition (7–8): $2s2p^3\ {}^3D_1$–$2s2p^3\ {}^3D_2$. (*a*) Collision strength versus energy relative to the Fe^{20+} ground state (this paper). (*b*) Effective collision strengths: solid curve, this paper; dashed curve, Butler and Zeippen (2000); dotted curve, Aggarwal (1991).

4.3. $n = 2$ to $n' = 4$

The only prior collision data involving the $n = 4$ levels are the distorted-wave results of Phillips *et al* (1996). In table 4, we compare collision strengths for those transitions $2s^22p^2\ {}^3P_1$–$2s^22p4d$ for which Phillips *et al* (1996) tabulated results to at least two significant figures. We observe no significant differences. The spacing of the $n = 4$ levels means that, in general, we expect little resonant enhancement of the effective collision strengths, except at low temperatures. However, the main motivation for including these levels was to obtain a consistent and comprehensive set of data that could be used for modelling the soft x-ray region.

4.4. All transitions

So far, we have focused on those transitions for which data already exist so as to make specific comparisons. In figure 9 we give a broad overview of our results, namely effective collision strengths at 10^7 K for all 19 900 inelastic transitions. The transitions are indexed according to the upper level changing most rapidly. A few broad features are evident: firstly, transitions from the $n = 2$ configurations span the first $\approx$4000 transitions (actually, 3790) and the 'hole'

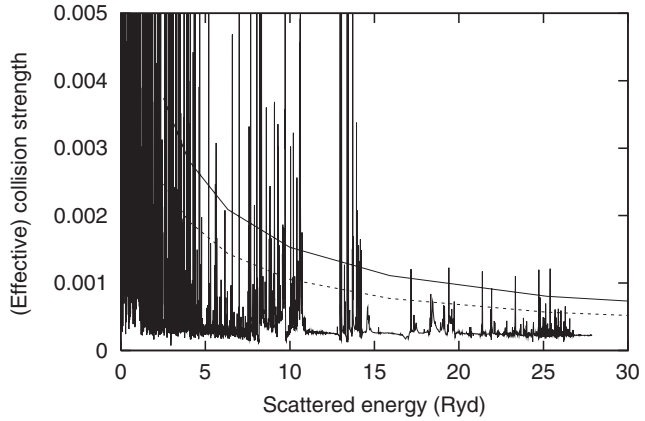

Figure 7. Transition (1–21): $2s^2 2p^2\ ^3P_0$–$2s^2 2p3s\ ^3P_0$. Collision strength versus energy relative to the upper level (this paper). Effective collision strengths versus temperature in Ryd: solid curve, this paper; dashed curve, Butler and Zeippen (2000).

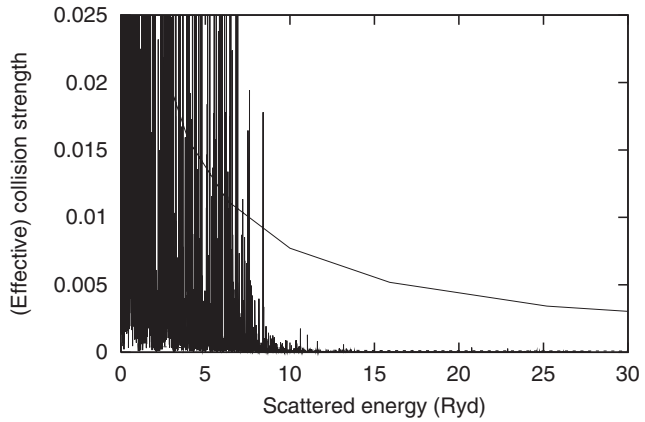

Figure 8. Transition (7–22): $2s2p^3\ ^3D_1$–$2s^2 2p3s\ ^3P_1$. Collision strength versus energy relative to the upper level (this paper). Effective collision strengths versus temperature in Ryd: solid curve, this paper; dashed curve, Butler and Zeippen (2000).

indicated is due to our omission of the $2p^3 3l$ configurations from our CC expansion. This means that we omit transitions of the form $2p^4 \rightarrow 2p^3 3l$, which would give rise to a set of relatively strong effective collision strengths, but do include relatively weak transitions of the form $2p^4 \rightarrow 2s2p^2 3l$ etc. Effective collision strengths for transitions from the $n = 3$ levels start to fall-off slightly above transition index $\approx$12 000, which is where transitions from the $2s2p^2 3l$ configurations start—we have omitted $2s \rightarrow 2p$ promotions from this configuration. Effective collision strengths for those transitions labelled $n = 4$ (from 19 160 and upwards) are relatively strong compared to those involving $n = 2$ and 3 levels. The reason for this is that an $n = 4$ electron interacts less with the core than, say, an $n = 3$ electron and the corresponding energy levels are more degenerate and, hence, the effective collision strengths between them are relatively larger.

Table 4. Collision strengths in Fe^{20+} from level 2 to levels of the $2s^2 2p4d$ configuration. For each transition, the first row is from Phillips *et al* (1996) and the second from our 200CC ICFT *R*-matrix calculation.

		Energies (Ryd)		
Upper-level index[a]	Level[b]	110	220	330
171	$^3F_2$	0.0016	0.0010	0.0010
		0.0014	0.0009	0.0009
172	$^3D_2$	0.0132	0.0202	0.0250
		0.0132	0.0195	0.0240
174	$^3D_1$	0.0028	0.0027	0.0031
		0.0027	0.0026	0.0029
186	$^1D_2$	0.0051	0.0077	0.0095
		0.0050	0.0073	0.0090
188	$^3P_1$	0.0057	0.0091	0.0114
		0.0057	0.0087	0.0108
189	$^3P_2$	0.0029	0.0037	0.0044
		0.0028	0.0034	0.0041
190	$^3P_0$	0.0024	0.0039	0.0049
		0.0024	0.0038	0.0047

[a] As labelled in the *adf04* file.
[b] Some of the spin-multiplicity labels given here differ from those in Phillips *et al* (1996).

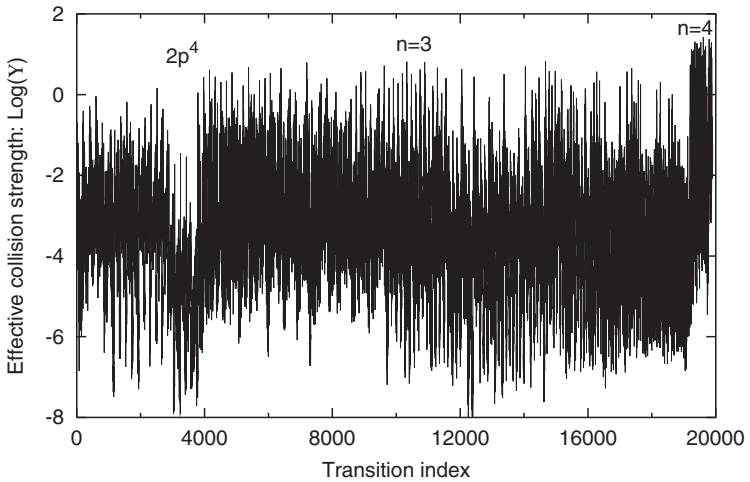

Figure 9. Effective collision strengths at a temperature of 10^7 K for 19 900 transitions in Fe^{20+}. The transition index (n) for the i–j transition is given by n: $j = i + 1, 200$, $i = 1, 200$ where i denotes the lower level and j denotes the upper level.

5. Conclusion

We have carried out a 200 level CC calculation for Fe^{20+} using the *R*-matrix method in conjunction with the ICFT method. We have generated effective collision strengths for all 19 900 inelastic transitions, which is an order of magnitude larger than has been generated hitherto. We find a broad accord with the (much smaller) set of data generated by Butler and Zeippen (2000), using the Breit–Pauli *R*-matrix method, as part of the IRON Project. As

expected, the main discrepancies arise on weak transitions where the additional resonance contributions that we provide for become paramount. This becomes more apparent for transitions from the first excited configuration than from the ground configuration. The consistent and comprehensive set of data that we have generated (energy levels, radiative rates and effective collision strengths) is necessary for the collisional–radiative modelling of metallic impurities that will arise in the next generation of magnetic fusion reactors as well as being of relevance to studies utilizing observations made by the high-resolution x-ray satellites *Chandra* and *XMM–Newton*.

Acknowledgments

In this paper, NRB was supported by a UK PPARC Grant (PPA/G/S/1997/00783) with the University of Strathclyde and DCG was supported by a US DoE Grant (DE-FG02-96-ER54367) with Rollins College. The computational work was carried out, in part, at the National Energy Research Center at Lawrence Berkeley National Laboratory.

References

Aggarwal K M 1991 *Astrophys. J. Suppl.* **77** 677–96
Aggarwal K M, Deb N C, Keenan F P and Msezane A Z 2000 *J. Phys. B: At. Mol. Opt. Phys.* **33** L391–401
Aggarwal K M, Hibbert A, Keenan F P and Norrington P H 1997 *Astrophys. J. Suppl.* **108** 575–90
Aggarwal K M and Keenan F P 1999 *J. Phys. B: At. Mol. Opt. Phys.* **32** 3585–99
Arnaud M and Raymond J 1992 *Astrophys. J.* **398** 394–406
Badnell N R 1986 *J. Phys. B: At. Mol. Phys.* **19** 3827–35
——1997 *J. Phys. B: At. Mol. Opt. Phys.* **30** 1–11
Berrington K A, Eissner W B and Norrington P H 1995 *Comput. Phys. Commun.* **92** 290–420
Burgess A 1974 *J. Phys. B: At. Mol. Phys.* **7** L364–7
Burgess A, Chidichimo M C and Tully J A 1997 *J. Phys. B: At. Mol. Opt. Phys.* **30** 33–57
Burgess A, Hummer D G and Tully J A 1970 *Phil. Trans. R. Soc.* A **266** 225–79
Burgess A and Tully J A 1992 *Astron. Astrophys.* **254** 436–53
Burke P G and Berrington K A 1993 *Atomic and Molecular Processes—an R-Matrix Approach* (Bristol: Institute of Physics Publishing)
Burke P G, Burke V M and Dunseath K M 1994 *J. Phys. B: At. Mol. Opt. Phys.* **27** 5341–73
Burke V M, Burke P G and Scott N S 1992 *Comput. Phys. Commun.* **69** 76–98
Butler K 2000 Private communication
Butler K and Zeippen C J 2000 *Astron. Astrophys. Suppl.* **143** 483–9
Corliss C and Sugar J 1982 *J. Phys. Chem. Ref. Data* **11** 135–241
Eissner W, Galavís M E, Mendoza C and Zeippen C J 1999 *Astron. Astrophys. Suppl.* **137** 165–73
Gorczyca T W and Badnell N R 2000 *J. Phys. B: At. Mol. Opt. Phys.* **33** 2511–23
Gorczyca T W, Robicheaux F, Pindzola M S, Griffin D C and Badnell N R 1995 *Phys. Rev.* A **52** 3877–88
Griffin D C and Badnell N R 2000 *J. Phys. B: At. Mol. Opt. Phys.* **33** 4389–408
Griffin D C, Badnell N R and Pindzola M S 1998 *J. Phys. B: At. Mol. Opt. Phys.* **31** 3713–27
Griffin D C, Badnell N R, Pindzola M S and Shaw J A 1999 *J. Phys. B: At. Mol. Opt. Phys.* **32** 2139–52
——1999 *J. Phys. B: At. Mol. Opt. Phys.* **32** 4129–31
Hummer D G, Berrington K A, Eissner W, Pradhan A K, Saraph H E and Tully J A 1993 *Astron. Astrophys.* **279** 298–309
Pelan J C and Berrington K A 2001 *Astron. Astrophys.* **365** 258–65
Phillips K J H, Bhatia A K, Mason H E and Zarro D M 1996 *Astrophys. J. Suppl.* **466** 549–60
Scott N S and Burke P G 1980 *J. Phys. B: At. Mol. Phys.* **13** 4299–314
Seaton M J 1953 *Proc. R. Soc.* A **218** 400–16
Summers H P 1994 *JET Joint Undertaking Report* JET-IR(94)06
——1999 *ADAS User Manual Version 2.1* webpage http://adas.phys.strath.ac.uk
Zhang H L and Sampson D H 1996 *At. Data Nucl. Data Tables* **63** 275–314
——1997 *At. Data Nucl. Data Tables* **65** 183–271